Structural assessment of late Neolithic *Sa Covaccada* Dolmen, Sardinia, Italy

Stefano De Santis

Roma Tre University

Department of Civil, Computer and Aeronautical Engineering

Via Vito Volterra 62, 00146, Rome, Italy

E: stefano.desantis@uniroma3.it | T: +39 06 5733 6387

ORCID: 0000-0002-0816-4865

ABSTRACT

The application of structural engineering tools to archaeological sites is unusual, while architects, archaeologists, and restorers are more commonly involved in these scenarios. Nevertheless, it can provide valuable indications for conservation and repair. This paper presents the structural assessment of the late Neolithic *Sa Covaccada* Dolmen, in Sardinia, Italy, regarded as a *unicum* in the Region and one of the most important megalithic monuments in the Mediterranean area. Due to severe material deterioration and extensive crack pattern, structural stability is a primary concern, yet it has not been assessed to date. To address this, both analytical rigid body analyses and 2D and 3D discrete element simulations were performed, contributing to an as challenging as fascinating multidisciplinary restoration project.

Keywords: Discrete Element Method (DEM); Archaeological site; Rigid body analysis; Mechanism method; UDEC; 3DEC.

1. INTRODUCTION

Structural engineers rarely deal with the assessment of archaeological monuments. On the one hand, archaeological sites are a niche area of investigation, due to their limited number and strong protection restrictions. On the other hand, they are traditionally prerogative of architects, archaeologists, and restorers, who are culturally regarded as closer and more trained than engineers in this field. Nonetheless, structural assessment and retrofitting are often needed, requiring engineering skills to participate in the work with the other experts. And even if archaeological sites do not play a central role in their academic education, structural engineers master the tools for expertly contributing to restoration projects.

Indeed, some applications of structural assessment to archaeological monuments are described in the literature. Türer and coauthors (Türer et al. 2012) used finite elements, whose elastic parameters were calibrated on small vibration monitoring, to perform reverse engineering on Nemrut Dağ Tumulus (Southeastern Anatolia, Turkey, I Century BC). They also correlated the damage state exhibited by cyclopic squared stone units and colossal statues with possible causes, including material degradation (due to stress concentrations and erosion), past earthquakes (the area is highly seismic), foundation settlements, snow pressure, wind load, and blasting (possibly used to explore the burial chamber in the inner core of the tumulus). Analytic studies were carried out by Reinosa and Romera (2015), based either on Coulomb Theory or on Log Spiral Theory with kinematic approach. An easy-to-use computational tool was developed to evaluate the overturing stability of megalithic orthostats, including the effects of wind and earth pressure, and was applied to the Dolmen of Dombate (Galicia, Spain, first half of IV Millenium BC) and to Champ Dolent Menhir (Brittany, France, V Millenium BC). Numerical simulations were used by Motsa and coworkers (Motsa et al. 2020) to perform eigenmode and non-linear static analyses of megalithic Mnajdra Prehistoric Temples (Malta, IV-III Millenium BC), with finite element models calibrated on ambient vibration monitoring.

They also investigated the sensitivity of mode shapes and frequencies to the properties of stone-to-stone contacts, highlighting the influence of joint properties.

The assessment strategies developed in the papers cited above have resorted to continuous formulations (finite elements). Nonetheless, in the light of the remarkable role played by discontinuities in the response of massive dry joint stone masonry assemblages, concentrated nonlinearities were introduced (Motsa et al. 2020). As an alternative, inherently discontinuous modelling approaches have been proposed, such as the Discrete Element Method (DEM), which makes use of rigid or elastic discrete blocks separated by discontinuities and interacting at contact points, which house strength properties. A numerical approach of DEM, named as Distinct Element Method, was originally developed for large scale analyses of fractured rock masses (Cundall 1971). Thanks to its accurate representation of discontinuous systems, it was then advantageously applied also to masonry structures (see, amongst others: Azevedo et al. 2000; Lemos 2007; Pulatsu et al. 2016; Bui et al. 2017). The explicit integration of the equation of motion makes the method computationally efficient for time-history analyses, and DEM has been profitably used for seismic assessment (Dimitri et al. 2011; de Felice 2011; DeJong and Vibert 2012; Canizzaro and Lourenço 2016; Meriggi et al. 2019). More recently, the evolution of modelling strategies and the advancement of computational performances has promoted the application of three-dimensional DEM. Pioneering works were published by Psycharis et al.(2011) and by Young et al. (2015) for the seismic assessment of antique large blocky structures. After that, 3D DEM was used in other studies (Psycharis et al. 2011; Lemos and Campos Costa 2017; Ferrante et al. 2021; Chen and Bagi 2023) with an increasing wealth, and complexity, of numerical models, which have moved on to include coupled fracture energy-based contact constitutive models (Pulatsu et al. 2021), to integrate 3D voronoi tessellation for automated mesh creation (Kassotakis et al., 2023), and to describe the torsion–shear behaviour of interlocking blocks (Mousavian et al. 2023).

As concerns archaeological monuments, DEM was used to simulate the earthquake response of ancient columns (Papantonopoulos et al. 2002) and investigate the correlation between the frequency content of seismic base acceleration and the occurrence of sliding or rocking between the blocks of multi-drum columns (Komodromos et al. 2008), using a specifically developed software validated against small-scale shake table tests. Psycharis and coworkers investigated the earthquake response of Parthenon (V Century BC) through, as said before, one of the very first structural applications of three-dimensional DEM (Psycharis et al. 2011). The seismic analysis of the Panhellenic Sanctuary of Nemea (northeastern Peloponnese, Greece, IV Century BC), which collapsed due to a destructive earthquake 2500 years ago, was carried out by Young and coworkers (Young et al. 2015) with 3D DEM, providing an insight on the dynamic response of dry stack stone masonry. The work showed the potential of discrete modelling approaches together with the importance of a careful characterization of unit and contact properties, and traced an outlook for DEM-based assessment and retrofit of antique masonry structures. Finally, Mordanova and de Felice (2020) applied DEM to the seismic assessment of the south-east external wall of the Colosseum (I Century AD), and of the Roman *opus reticolatum* / *opus quadratum* Claudio Aqueduct (Rome, Italy, I Century AD). Both push-over and non-linear time-history analyses were carried out on a simplified 2D geometry, although authors highlight that future research efforts should be devoted to the development of 3D DEM models that account for actual spatial geometry.

These latter studies have showed that using DEM can be beneficial for archaeological monuments, consisting of few gigantic stones with irregular geometry, interacting at concentrated locations, and exhibiting rigid body large movements. The current state of knowledge regarding structural assessment methods shows a diverse range of approaches, with no consensus on the most suitable methods.

This paper presents the structural analyses carried out on *Sa Covaccada* Dolmen, in Sardinia, Italy (illustrated in §2.1). The Dolmen dates to the late Neolithic (III Millenium BC) and is considered a *unicum* amongst the megalithic monuments in Sardinia, for both its size and its peculiar shape, as well as one of the most important ones in the Mediterranean area (Cicilloni 2009). Regrettably, the monument exhibits extensive local surface exfoliations, biodeterioration, bleaching, and biological colonisations, and a severe crack pattern, which makes structural stability a main concern (§2.2). To respond to urgent assessment needs, both analytical rigid body analyses (§4) and numerical simulations with DEM were carried out (§5). DEM analyses were performed both in 2D on relevant cross-sections (§5.1), and in 3D on a spatial model (§5.2), obtained from digital survey (§3.1). Joint properties were derived from material characterization tests (§3.2) and tuned based on surveyed contact surface areas. Structural assessment was part of a wider project involving architects, archaeologists, restorers, geologists, and biologists, which makes this work a virtuous example of the contribution of structural engineering tools to the multidisciplinary scenarios of archaeological restoration.

2. SA COVACCADA DOLMEN

2.1. Description of the structure

Sa Covaccada Dolmen is a megalithic monumental complex near Mores, Sassari, in the northern hinterland of Sardinia. The structure rests on a trachyte tableland and has a 5.00m×2.20m rectangular plan. It comprises two vertical stones (orthostats), one on the east and one on the west side, which are 1.95÷2.00m high, 0.48÷0.91m thick and are housed in shallow ditches excavated in the base stone. On top, the orthostats support a 0.61÷0.65m thick capstone, which originally must have covered the whole structure and only a portion of which has survived until today (Figures 1-2). The total height is about 2.70m. In the middle between

the orthostats and the top capstone there are small basalt stones, placed to flatten the surface (even if some of them may not be original). On the front side (south-east) there is an incomplete 0.35 thick stone, with a small (0.71m×0.51m) opening (Figure 1a), whereas the back (north-west) stone has been lost. The orthostat on the west side has a 0.50m deep niche, which is 1.22m high and 0.88 wide, suggesting that the structure had a sepulchral function. Since the niche was obtained by removing the material from the stone, the thickness of the orthostat behind it has been estimated as 18÷20cm only. The monument is built in grey-pink tuffaceous trachyte, an extrusive igneous soft rock, very porous and rich in phenocrystals of zeolite (clinoptilolite), smectite, feldspar, plagioclase, pumice and quartz fragments, immersed in an amorphous brown-grey vitreous matrix. Instead, as said before, the small stones serving as wedges between capstone and orthostats are in basalt.

The Dolmen, together with a Menhir laying on the ground about 100m apart broken in several portions, are the unique remains of a wide archaeological site located along an old transhumance track, dating back to the late Neolithic (3300-2800 BC). Its name, in the local old dialect, means "*covered*" or "*stone that covers*", which recalls its home-shape, as the monument was probably erected as a common grave tomb for important local people. The Dolmen is considered the most significant megalithic complex in Sardinia, and is acknowledged as an unvaluable testimony in the evolution of prehistoric sepulchral architectures in the area, as proved by the similarities of the niche and the opening with some features of pre-Nuragic *Domus de Janas* (fairy houses) tombs (V-IV Millenium BC), whilst the front stone is considered the precursor of the later Nuragic *Tombs of Giants* (II Millenium BC). *Sa Covaccada* Dolmen is an *unicum* amongst the megalithic monuments in Sardinia, for both its size and its peculiar shape, but shows remarkable analogies with the Dolmens in Ala Safat, West Bank, and in Coste Rouge-Hérault, France, providing evidence of the circuits Sardinia was part of in Chalcolithic

(III Millenium BC) (Cicilloni 2009). *Sa Covaccada* Dolmen, together with the Menhir nearby, is included in the tentative list submitted to UNESCO for recognition as a World Heritage Site.

2.2. Damage state and previous restoration works

The Dolmen exhibits severe deterioration. From a structural standpoint, the extensive crack pattern raises concern. Through-cracks, with maximum detectable width of 10.9÷24.2cm, divide the capstone in five distinct portions (labelled from C1 to C5 in Figures 1b and 2d,f), or, more precisely, the remaining part of it on the front side, since, as said before, its back portion has fallen and got lost. These five portions slightly moved with respect to each other, rotating with different angles around their respective supports, resulting in a loss of alignment. The lateral orthostats present several subvertical through-cracks (Figures 2a,c) and the front stone is cracked as well (Figures 2b,e). Fractures on vertical blocks have a maximum thickness of 2.9÷4.2cm for the east orthostat, of 2.5÷7.8mm for the west orthostat, and of 1.9÷6.2cm for the front stone. They all appear to be due to overloading (the compressive strength was overcome locally), because their layout, converging toward the small stone wedges, indicate a correlation with stress concentrations (Türer et al. 2012). Their rounded corners suggest they are old, but their age cannot be determined precisely (Martinez-Torres 2017).

Hair-cracks and flake debonding are visible over nearly all the surface, which may be attributed to wind erosion (Cassar et al. 2011), wet-dry cycles (Torpiano 1995) caused by rain fall and sun exposure (the stone has a high moisture absorption capacity at the molecular scale, Islam and Mohr 2023), and thermal cyclic stresses (Cassar et al. 2018), and may locally reduce the strength of the material. Finally, a dark patina rich in phosphorus (probably due to wood combustion), biological colonization (mosses and lichens) and chromatic alterations due to animal waste were surveyed.

In 2011, the monument underwent restoration works. First, a provisional roof was built, and the area was fenced. The deterioration was surveyed, and some small stones collected inside the Dolmen were removed and stoked in the vicinity, documenting the movement. Then, the stone surface was consolidated by nebulizing ethyl silicate, and biocide solutions were applied to remove biological colonisations. The portions of the capstone were re-aligned using actuators, and provisional steel supports were installed to prevent further movements and collapses. To the same end, wood wedges were inserted between the capstone and the orthostats. Since then, steel supports have been removed and wood wedges have dried, shrunk, and fallen. All the main cracks of the capstone, the orthostats, and the front stone were filled with epoxy resin mixed with fine trachyte power, sand, and pigments, to obtain a final colour similar to (but intentionally slightly lighter than) the original one and keeping an undercut to leave the restoration identifiable (Figures 2e-f). Finally, diffused consolidations were carried out to re-bond detached stone flakes, using the same epoxy resin leaked into the micro-cracks, also installing small metallic bars where needed.

Even if no signs of dangerous damage evolution have been reported in the last 12 years, experts agree that these interventions did not fully solve structural and conservation issues, and according to the Archaeological Authority, which is in charge of maintaining the monument, there was the need of assessing the structural stability, completing the restoration works, removing provisional equipment, and arranging the area for the cultural and touristic exploitation it deserves.

3. FIELD AND LABORATORY INVESTIGATIONS

3.1. Laser scan and photogrammetric survey

A detailed geometric survey of the Dolmen was conducted using laser scanning and digital photogrammetry. Images were taken from all around the monument, including from above, and both from outside and from inside. Care was taken to survey the basalt wedges, which was complicated by the small gap and the shadows. The crack pattern was narrowly surveyed as well. Frames were post-processed to build a 3D geometric model (Figure 3) with a resolution of 1mm, which was more than adequate for structural assessment (even if it is probably not enough, alone, for periodic crack monitoring). Clearly, the model only includes the outer surface of the stone blocks, whilst the actual crack path across their thickness and the exact depth of the bottom surface of the orthostats (the interface with the base stone) were undetectable. In addition to the main cracks, the other deterioration signs (hair cracks and local surface exfoliations, biodeterioration, bleaching, biological colonisations) were reported. The model could be explored and cut to extract 2D cross-sections (Figure 3) for structural analyses. Three vertical transversal sections, named as A-A', B-B', and C-C' (Figures 2, 3, and 4a-c), were extracted that include the capstone where it is cracked, the contact point between the two capstone portions separated by the crack, and the basalt wedges at the support interface between capstone and orthostats.

3.2. Mechanical characterization tests

A stone sample of the same lithotype of the Dolmen, with approximate size of 15cm×10cm×9cm, was collected in the field near the monument (Figure 5a) and delivered to the experimental laboratory of Roma Tre University in Rome. Its apparent density was measured as 1.8g/cm^3 according to (CEN 2006), and then it was cut with a numerically

controlled milling machine to extract three cubic specimens with 50mm edge (Figure 5b). Specimens were subjected to compression tests, performed as per (CEN 2007), using an MTS Universal testing machine with 100kN load capacity, under machine stroke displacement control at a constant rate of 0.005mm/s. The upper plate was provided with a spherical joint to accommodate possible imperfections in the planarity of the loaded faces of the specimen (Figure 5c). Integrated load cell and LVDT transducer measured load and displacement at 10Hz sampling rate. Stress was calculated by dividing the load by the surface area of the specimen, whereas strain was calculated by dividing the displacement by the height. Strain data derived from LVDT displacements were not considered reliable due to unavoidable settlements and possible localized displacements in the wedges of the testing machine, so they were corrected based on the measurements provided by digital image correlation (DIC). To apply DIC, the surface of the specimens was prepared with a speckle pattern made of black dots randomly distributed over a white background. A digital camera was placed on a stiff support at 46cm from the specimen and took pictures at 2s interval during test execution. Digital images had 6016px×4016px resolution, which corresponded to a pixel size of 35÷37μm and, thanks to the subpixel interpolation algorithm used for post-processing, to a resolution in the order of 1μm. Pictures were correlated with NCorr software, developed in Matlab® environment (Blaber et al. 2015), to derive displacement and strain fields (Figure 5d), and to calculate the strain values on the central portion of the specimen, thus excluding the areas near the loading plates where the stress and strain fields may be affected by friction induced confinement.

The resulting axial stress versus axial strain response curves are shown in Figure 6. The mechanical behaviour of the stone exhibited an initial linear branch up to about 70÷80% of the peak stress, followed by a non-linear pre-peak phase and a long post-peak softening. The average compressive strength resulted f_c=18.6N/mm^2 (Coefficient of Variation *CoV*=7%) and the average modulus of elasticity (secant value between 40% and 80% of fc) was

E_c=6.1kN/mm^2 (*CoV*=21%). More tests should be performed to improve the statistical significance of these mechanical properties, but the number of specimens was limited by the size of the stone unit collected in the field and delivered to the laboratory.

4. RIGID BODY ANALYSES

As a first step of the assessment, the collapse behaviour of the Dolmen was studied with a limit analysis approach. The three cross-sections A-A', B-B' and C-C' shown in Figure 4a-c were considered, assuming infinite compressive strength and stiffness of the material. Given the support provided by the orthostats to the capstone and the sub-vertical crack that divides the capstone in two separate stone units, the Dolmen was represented in a two-dimensional domain as a rigid-body mechanism. Under the forementioned assumptions, the blocks of the capstone can rotate with respect to each other around three pin hinges, located at the edges of the blocks, or at their actual contacts, and identified by points B (support of the east orthostat), C (support of the west orthostat), and O (contact point between the two capstone portions separated by the crack). The unique load considered was the self-weight, since possible loads due to wind, traffic, etc. cause insignificant effects and seismic load is negligible in the site (Meletti et al. 2008).

The structure turns into a mechanism when, in addition to the three hinges, a translation activates as well. This was considered to occur either at point B or at point C. By doing so, indeed, two possible collapse mechanism were considered. The first one was named as east mechanism, and involves the east orthostat (block I, Figure 7a) and the two blocks (II and III) of the capstone, whilst the right support of block III is fixed (Figure 7b). The second one was named as west mechanism and involves the west orthostat (block IV, Figure 7d) and the two blocks (II and III) of the capstone, and, this time, the left support of block II is fixed (Figure

7c). Therefore, the mechanism activates when the involved orthostat starts overturning, allowing the translation of the support.

To derive an estimate of the safety level of the Dolmen with respect to collapse, the self-weight of the capstone was multiplied by a load multiplier, calculated as that corresponding to the activation of the mechanism, and named as λ_E for the east mechanism and λ_W for the west mechanism.

When turned into a mechanism, the structure can be studied as a single degree of freedom system, which means that all its generalized displacements (translations and rotations) can be expressed as a function of only one of them, chosen and the Lagrangian parameter of the mechanism (Erdman and Sandor 1984). The relationships between the generalized displacements and the equations for calculating the load multiplier are discussed in the following, considering the east mechanism (Figures 7a-b). Clearly, an analogous process could be repeated for the west mechanism.

Nomenclature is as follows: X_{BO} and Y_{BO} are the width and the height of block II; X_{OC} and Y_{OC} are the width and the height of block III; X_{II} is the horizontal distance of the centre of gravity of block II measured from point B; X_{III} is the horizontal distance of the centre of gravity of block III measured from point C; Y_{AB} and Y_{CD} are the heights of blocks I and IV; X_I is the horizontal distance of the centre of gravity of block I measured from point A; X_{IV} is the horizontal distance of the centre of gravity of block IV measured from point D; u and v are horizontal and vertical displacements; ψ is the rotation of block III with respect to the fixed support C and φ is the rotation of block II with respect to the movable support B (counterclockwise rotations are assumed as positive), W_I, W_{II}, W_{III}, and W_{IV} are the weights of blocks I, II, III and IV; and, finally, H_I is the horizontal force transferred to the east orthostat by the capstone at point B, and H_{IV} is the horizontal force transferred to the west orthostat by the capstone at point C.

The boundary conditions are established by Eq. 1, in which v_B is the vertical displacement of point B and u_C and v_C are the horizontal and vertical displacements of point C; the congruence conditions are represented by Eq. (2), containing the horizontal and vertical displacements of point O, which is seen as a vertex either of block II ($u_{O,II}$ and $v_{O,II}$) or of block III ($u_{O,III}$ and $v_{O,III}$).

$$v_B = 0;\ u_C = 0;\ v_C = 0 \tag{1}$$

$$u_{0,II} = u_{0,III};\ v_{0,II} = v_{0,III} \tag{2}$$

The displacements of Eq. 2 are calculated using the first order theory as shown in Eqs. 3-4 and then Eq. 5 is obtained from the congruence conditions.

$$\begin{cases} u_{O,II} = -u_B + \varphi \cdot Y_{BO} \\ v_{O,II} = -\varphi \cdot X_{BO} \end{cases} \tag{3}$$

$$\begin{cases} u_{O,II} = \psi \cdot Y_{OC} \\ v_{O,II} = -X_{OC} \end{cases} \tag{4}$$

$$\begin{cases} \varphi = \frac{X_{OC}}{X_{BO}} \\ u_B = Y_{OC} + \varphi \cdot Y_{BO} = Y_{OC} + \frac{X_{OC}}{X_{BO}} \cdot Y_{BO} \end{cases} \tag{5}$$

Eq. 6 lists the virtual displacements of the points of applications of forces λW_{II}, λW_{III} and H_I. Note that the equations provide the displacement components in which the forces spend work, that is, the vertical displacements for self-weights W_{II} and W_{III} and the horizontal one for the thrust H_I.

$$\begin{cases} v_{\mathrm{II}} = -X_{II} \cdot \varphi = x_{\mathrm{II}} \cdot \frac{X_{OC}}{X_{BO}} \\ v_{III} = -X_{III} \\ u_B = Y_{OC} + \frac{X_{OC}}{X_{BO}} \cdot Y_{BO} \end{cases} \tag{6}$$

For the considered mechanism depicted in Figure 7b, the vertical loads W_{II} and W_{III} play a tilting role and spend a positive work (named as external work, W_{EXT}) in the vertical

displacements v_{II} and v_{III}, whereas the horizontal thrust H_I plays a stabilizing effect and spends a negative work (resisting work, W_{RES}) in the horizontal displacement u_B. The principle of virtual works states the equivalence between the resisting work and the external work multiplied by λ_E (Eq. 7). The load multiplier of the east mechanism λ_E (Eq. 8) is attained when the external work equals the maximum resisting work, that is, when H_I attains the value that makes the east orthostat (block I) overturn (Eq. 9).

$$\lambda_E \cdot W_{EXT} - W_{RES} = 0 \Rightarrow \lambda_E \cdot \left[W_{II} \cdot \left(X_{II} \cdot \frac{X_{OC}}{X_{BO}}\right) + W_{III} \cdot X_{III}\right] = H_I \cdot \left(Y_{OC} + \frac{X_{OC}}{X_{BO}} \cdot Y_{BO}\right) \quad (7)$$

$$\lambda_E = \frac{H_I \cdot \left(Y_{OC} + \frac{X_{OC}}{X_{BO}} \cdot Y_{BO}\right)}{\left[W_{II} \cdot \left(X_{II} \cdot \frac{X_{OC}}{X_{BO}}\right) + W_{III} \cdot X_{III}\right]} \quad (8)$$

$$H_I = \frac{W_I \cdot X_I}{Y_{AB}} \quad (9)$$

This approach was applied to the east and west mechanisms of the three cross-sections, as shown in Figures 4a-c, considering their simplified geometry as depicted in Figures 4d-f, in which the edges of the stone units were slightly regularized to segmental polylines, taking care to keep the mismatch with the surveyed geometry below 5% for volume (and, therefore, mass), and position of centres of gravity, while keeping unmodified the exact position of contact points, including those between orthostats and foundation. The resulting collapse multipliers λ_E and λ_W are listed in Table 1.

In all cases, load multipliers were estimated as higher than 1, meaning that the monument is in safe equilibrium conditions according to the applied mechanism method. Obviously, since the Dolmen is standing, a load multiplier λ<1 would have indicated that some features contributing to its stability had been incorrectly disregarded in the analysis. The east mechanisms resulted weaker (λ_E=2.0÷2.3) than the west ones (λ_W=5.3÷6.1) in all the three sections, suggesting that if a collapse occurred, this would involve the east orthostat, rather than the west one, in addition to the capstone. This was due to the larger resisting moment of the

west orthostat, whose base hinge (identified as point D in Figures 7d and 8d-f), has a larger eccentricity with respect to the centre of gravity, if compared to the resisting moment of the east orthostat and its base hinge (Point A in Figures 7a and 8a-c).

Finally, it is worth noting that the problem under study is unusual, because rigid block analysis is more often used to investigate the response of masonry structures under self-weight vertical loads, which spend most of the resisting work, and horizontal forces, calculated as the product of self-weight and load multiplier, which generally represent seismic actions and spend most of the external work (Oppenheim 1992; Clemente 1998; De Santis and de Felice 2014). In the present case, instead, possible collapse mechanisms are activated by the self-weight and no other loads are considered on the structure.

5. DISCRETE ELEMENT ANALYSES

The Discrete Element Method (DEM) models the structure as an assembly of discrete blocks, which may be either rigid or deformable, and interact at zero-thickness interfaces. Block corners house contacts, which feature stiffness and strength properties through normal and shear non-linear springs. Displacements are concentrated at these discontinuities. The resolution scheme is based on the explicit integration in the time domain of the equation of motion of each block, which makes DEM computationally efficient for dynamic/seismic analyses. Moreover, it allows reproducing the effective shape and arrangement of units, models crack opening and joint sliding, and automatically updates block position and contacts, allowing large displacements and rotations.

For DEM simulations, the stone units of the Dolmen were defined based on geometric survey, including stone shapes, contact points, and crack pattern, and were assumed as rigid. Normal springs were considered as elastic with infinite strength in compression and no tensile

strength, whilst an elastic perfectly plastic constitutive relationship was assumed for shear springs, considering a Coulomb failure criterion with friction angle φ and no cohesion.

5.1. 2D DEM analyses

5.1.1. Geometry and mechanical properties of the model

Two-dimensional discrete element simulations were carried out using UDEC® (Universal Distinct Element Code) commercial software (Itasca 2011). The three sections extracted from the surveyed 3D geometrical model and represented in Figures 4a-c were analysed. Their simplified geometries depicted in Figures 4d-f were considered, as in the rigid body approach described in §4 and were semi-automatically imported in UDEC as lists of coordinates through a FISH programming language routine.

Each unit, named as I, II, III, and IV, was modelled as a rigid block. Self-weight density was calculated as the measured unit weight of trachyte (18kN/m^3, §3.2) multiplied by the thickness in the third direction, the one normal to the plane of the analysis, as listed in Table 2. Additionally, to provide the model with boundary conditions, a fully fixed base block was defined, which was considered as rigid and provided with the same mass density of the other ones (even if mass is irrelevant in this case).

Block corners were rounded with a radius equal to 1% of block length (Itasca 2011) to provide numerical stability, allow the definition of normal and tangential vectors at the corners, and account for the limited compressive strength, which makes the development of hinges at the edge of a block impossible.

The elastic stiffness in compression of the normal springs (k_n) was calculated for each contact point based on the experimentally determined Young's modulus of trachyte (E_c=6.1kN/mm^2, §3.2), the size of the two blocks in contact, and the effective surveyed contact surface area (Mordanova and de Felice 2020). It varied between $3.1 \cdot 10^9$Pa/m and $9.7 \cdot 10^9$Pa/m,

except for the two blocks (II and III) of the capstone separated by the subvertical crack and in contact over a smaller surface than elsewhere, where k_n=0.9÷1.0·10^{8}Pa/m. As for the shear springs, the stiffness, which could not be determined on measured data, was taken as equal to 0.5k_n. In the literature (Oliveira et al. 2012; Pappas, Da Porto and Modena 2016; Lemos and Campos Costa 2017; Sarhosis et al. 2019; Salvalaggio et al. 2021), it is recommended to assume k_s=0.5÷1.0k_n; in the present case, sensitivity analyses within this range indicated negligible differences in the resulting load multiplier at collapse. No tensile strength and cohesion were considered.

Finally, a friction angle φ=35° was taken, considering the irregular and rough surface of the real joints (Lemos and Campos Costa 2017), and based on the literature (Oliveira et al. 2012; Pappas, Da Porto and Modena 2016; Sarhosis et al. 2019; Salvalaggio et al. 2021). Sensitivity analyses in the φ=30°÷40° range showed a variation of the resulting load multiplier at collapse of less than ±10% with respect to that corresponding to φ=35°. Note that the exact geometry of the main cracks across the thickness of the stone blocks is undetectable today, since cracks were filled with epoxy resin, but documents on surveys carried out before this intervention were available.

5.1.2. Analyses and results

DEM analyses were performed in the time domain by explicit integration of the equations of motion. An incremental protocol was developed in FISH, in which a vertical acceleration equal to 0.4905m/s^2 (5% of gravity) was applied to the centre of mass of each block and progressively incremented. Quasi static conditions were obtained through a local artificial viscous damping coefficient of 0.8 (Itasca 2011) and the resolution procedure passed from one step to the following one only after static equilibrium was achieved. Thus, after 20 steps the gravity was fully applied, but simulations were continued until collapse, which was attained by the loss of equilibrium, that is, the displacement of one block (or more blocks) diverged. The

load multiplier λ was then calculated as the vertical acceleration attained at failure divided by gravity. Noteworthy is that only one multiplier was determined for each cross-section, since in DEM simulations all the blocks were possibly involved in the mechanism and splitting the analysis in two subcases, as in the analytical rigid body analyses, was unnecessary.

The load multipliers, listed in Table 1, resulted slightly lower than those provided by rigid body analyses, which was due both to the deformability of contacts, which were implicitly assumed as infinitely rigid in the analytical approach, and to the possibility for all the four blocks to rotate. In other terms, the stronger constraint conditions assumed in rigid body analyses led to a higher load multiplier if compared to DEM simulations. It should be also considered that in DEM simulations, differently from analytical calculations, it was possible to amplify gravity in all the blocks, which entailed that an increase of the vertical load in the capstone corresponded to an increase of the capacity of the orthostats against overturning.

The displacement configurations at the last step before collapse, shown in Figure 9, indicate that estimated collapse involved mainly the east orthostat and the capstone, whilst the west orthostat exhibited negligible displacements, consistently with the outcome of rigid body analyses, which provided lower load multipliers for the east mechanism (λ_E) with respect to the west mechanism (λ_W). Finally, no sliding was predicted at the joints by numerical simulations, which was consistent with the absence of any signs of slippage surveyed on the Dolmen.

5.2. 3D DEM analyses

5.2.1. Geometry

Three-dimensional discrete element simulations were carried out using 3DEC® commercial software (Itasca 2020). Differently from the 2D analyses, the definition of geometry required some pre-processing. First, the external surface of the monument provided by digital survey was imported as a stereolithography (also named as Standard Tessellation Language, STL) file

in Autodesk Meshmixer® software (Figure 10a). STL approximates the geometry of a surface with a mesh of triangular elements and saves information in a binary file, much smaller than an ASCII file, saving space and run time. Then, surfaces were divided according to the surveyed geometry of stone units and closed. The shape and position of the basalt wedges, which were not closely detected by digital survey, were refined at this stage. Autodesk Meshmixer® provides a simplified, smooth, continuum and non-self-intersecting mesh by controlling solid accuracy and mesh density according to a minimum voxel (volumetric picture element) size criterion (Figure 10b). In the present case, referring to the east orthostat shown in Figure 10 only, the initial STL model from geometrical survey had 860,463 nodes and 1,720,910 triangles, whereas the simplified mesh built in Autodesk Meshmixer® had 25,443 nodes and 50,882 triangles. Finally, the mesh was imported in 3DEC® and blocks were created (discretized in 6995 3D elements for the east orthostat, Figure 10c).

An alternative method was investigated using Rhino3D®, instead of Autodesk Meshmixer®. The shapes of the blocks were enveloped and a slightly simplified with an approximating surface, which was then meshed to reduce mesh complexity (number of triangular surface elements and nodes). Finally, STL meshed surfaces were imported in 3DEC®, which operated a further geometrical simplification, created blocks (one block for each closed surface imported from Rhino3D®), and finally meshed them. Nonetheless, this method was less precise than the one with Autodesk Meshmixer®, due to the use of an approximating envelope surface, and led to a larger number of blocks in the 3DEC® model with a consequent higher computational effort.

Both pre-processing strategies with Autodesk Meshmixer® and Rhino3D® allowed the definition and the analysis of concave blocks. This would have been unfeasible if the geometry was imported directly in 3DEC®, which requires convex surfaces to import geometry, generate blocks and create mesh. The blocks were cut to introduce the crack pattern of the front stone (Figure 11a), of the capstone (Figure 11b) and of the two orthostats (Figures 11c,d). To this

aim, cut planes were defined in Autocad® and imported in 3DEC®, and then recalled in the code. The rounding of crack edges was also represented in the model since it affects the actual position of the hinges.

Finally, a fully fixed base block was defined to provide the model with a boundary condition, like in the 2D DEM simulation.

5.2.2. Mechanical properties

A mass density of 18kN/m^3 was assigned to the blocks, which were modelled as infinitely rigid. Joints were modelled as non-linear contacts, provided with an elastic stiffness in compression (k_n) and in shear k_s=0.5k_n. The compressive stiffness was determined based on the size of the blocks, on the Young's modulus of the stone (§3.2), on the relationships provided by the literature (Lourenço et al., 2005), and on the values considered by other authors for dry stone masonry (Oliveira et al., 2012, Sarhosis et al., 2019). It resulted $0.34 \cdot 10^9$Pa/m for the capstone, $0.14 \cdot 10^9$Pa/m for the west orthostat and $0.20 \cdot 10^9$Pa/m for the east one, $0.43 \cdot 10^9$Pa/m for the front stone, $1 \cdot 10^9$Pa/m for the basalt wedges and, finally, $0.35 \cdot 10^9$Pa/m for the joint between orthostat and base block.

As for the failure conditions, the compressive strength was set as unlimited, whereas an elastic-plastic constitutive relationship was considered in shear, using a Coulomb criterion with a friction angle φ=35°, no cohesion and no tensile strength (as in the 2D DEM model).

5.2.3. Analyses and results

Analyses were performed in the time domain, by incrementing the vertical acceleration by 0.05g steps with a protocol developed in FISH. An artificial viscous damping coefficient of 0.8 was used to run quasi-static analyses (Itasca, 2020). Numerical simulations estimated the load multiplier (λ_{3D}) as the total vertical acceleration at collapse divided by the gravity. To limit runtime, a maximum number of 120 cycles was set, after which collapse was not attained, which

corresponded to a load multiplier higher than 6. Small block displacements were recorded, which increased nearly linearly with time and did not exhibit any signs of divergence (Figure 12a). They suggested that the irregular crack pattern of the capstone made its blocks interlock. Moreover, the weight of the largest capstone unit (C5, the one at the back of the monument) had a stabilizing effect on the east orthostat (the one involved in the failure mode predicted by 2D DEM). Finally, friction made the capstone behave as a tie in that area, increasing the capacity of the orthostats against overturning. The combination of these factors enhanced the estimated safety level with respect to previous analytical and numerical analyses, which focussed on transversal cross-sections with a crack in the capstone and, therefore, were unable to consider such eminently three-dimensional behaviour.

To confirm these observations, 3D DEM simulations were repeated excluding the large capstone unit C5. The estimated load multiplier resulted equal to 1.9, as after 38 cycles displacements exhibited a clear deviation from the linear trend, indicating the activation of a collapse mechanism (Figure 12b). Interestingly, such mechanism involved units C1, C2 and C3 of the capstone and the east orthostat (Figure 13), which did not correspond to any of the mechanisms investigated with 2D analyses, in which either C1 and C2 (section A-A', Figure 4a) or C3 and C4 (sections B-B' and C-C', Figures 4b-c) were considered.

CONCLUSIONS

The *Sa Covaccada* Dolmen in Sardinia, Italy, from the advanced stages of the Neolithic era, displays significant crack pattern and material deterioration. Even if restoration interventions were carried out in 2011, apprehensions persist about its stability. This made structural assessment needed within a broad restoration project involving experts in archaeology, architecture, biology, and geology.

It can be inferred that cracks were due to excessive loading, and their rounded borders indicate their antiquity, even if it is impossible to state how old they are. They have divided the capstone into five blocks and the primary concern regarding overall structural safety now stems from equilibrium issues. Structural assessment opted for inherently discontinuous approaches that closely represented the complex geometry of the stone blocks and allowed large displacements to be considered at crack interfaces. The possible onset of collapse mechanisms was studied, involving the blocks of the capstone separated by a crack and one of the two orthostats or both.

Following a detailed digital survey and laboratory investigations for the mechanical characterization of the trachyte of the Dolmen, the structural condition was assessed both analytically, through limit analysis, and numerically, with discrete element (DEM) simulations. The safety level was estimated through a load multiplier that amplifies the self-weight, which is the unique significant load, since wind, environmental noise and earthquake have negligible effects. The outcomes provided by the different methodologies were only partially consistent.

For 2D analyses, relevant transversal cross-sections were considered that included a through-crack in the capstone. In the mechanism method, the self-weight of the capstone was amplified, and the maximum thrust the orthostat can carry on top before overturning was assumed as a limit condition. The principle of virtual works provided separate load multipliers for collapse mechanisms involving either the east orthostat or the west one, ranging between 2.0 and 2.3 and between 5.3 and 6.0, respectively. Two-dimensional DEM simulations led to load multipliers in the 1.2÷1.5 interval for the three cross-sections. The lower load multipliers provided by DEM if compared to the mechanism method were attributed to the deformability of contacts and to the possibility for all the four blocks to rotate, corresponding to weaker constraint conditions.

For the considered cross-sections, both analytical computations and numerical simulations suggested that any potential collapse would involve the east orthostat rather than the west one, which has a larger width at the base, yielding a higher capacity against overturning.

Three-dimensional DEM analyses were carried out on a model built from digital survey that reproduced spatial geometry and crack pattern. Outcomes showed the interlocking provided by the irregular layout of cracks, the stabilizing effect on the east orthostat of the weight of the largest and uncracked capstone unit and its contribution in limiting overturing associated with friction at its interface with the orthostats. The load multiplier resulted higher (larger than 6) that the ones estimated by 2D analyses, which neglected three-dimensional behaviour and, therefore, disregarded their contribution to the safety of the monument.

Despite such differences, load multipliers indicated that the structure is in safe conditions according to the applied methods. Derived from these results, there is no urgency for immediate actions. Works to undertake for improving the state of the Dolmen include expanding the contact area between the capstone and orthostats by introducing additional wedge stones to mitigate stress concentrations and prevent further damage. This may require that the capstone is lifted, to ensure that the new wedges effectively carry the load, but deeper analyses are needed to design an appropriate setup for this delicate operation. The new stones will be placed on the entire length of the orthostats, near the internal edge of their tup surface, to reduce the external work and increase the resisting work, increasing the safety level according to analytical calculations.

Regular monitoring of the crack pattern will be implemented to promptly identify potential changes and a suitable technology will be identified to this end. Due to the restrictions to installing permanent instruments, and the risk that sensors are damaged or stolen, temporary markers could be attached with reversible adhesive and used for (bi)yearly measurements with digital deformometer and/or high-resolution image-based techniques. Crack monitoring could

reveal the necessity for immediate intervention, which may include temporary supports, tie-bars, or buttresses, to be removed after definitive retrofitting. DEM models will be updated if new cracks are detected. Additionally, the stones will be locally consolidated, their surfaces will be cleaned from dirt patinas, and biological colonisations will be removed. The temporary roof will be substituted with a new one integrated within the landscape, to return the Dolmen of *Sa Covaccada* to local and global communities and promote its safe cultural fruition.

DECLARATION OF INTEREST STATEMENT

The author declares that there is no known competing financial interests or personal relationships that could have appeared to influence the work reported in this paper.

ACKNOWLEDGEMENTS

This study is part of a wider interdisciplinary project coordinated by Carla Tomasi (architect) and in cooperation with the experts Angela Savalli (restorer), Ornella Salvadori (biologist), Alessandro Massa (architect), Lorenzo Lazzarini (geologist), and Lorenzo Poggi (geologist), whose advice was professionally fruitful and culturally enchanting. The support of Segretariato Regionale del Ministero della Cultura per la Sardegna (Patrizia Tomassetti, Secretary, Massimo Casagrande, RUP, Pina Corraine, archaelogist, and Charlotte Montanaro, restorer) is kindly acknowledged.

REFERENCES

Azevedo, Joao J., Gabriela Sincraian and José V. Lemos. 2000. “Seismic behavior of blocky masonry structures.” *Earthquake Spectra* 16 (2): 337–365. https://doi.org/10.1193/1.1586116.

Blaber, Justin, Bemjamin S. Adair and Antonia Antoniou. 2015. "Ncorr: Open-Source 2D Digital Image Correlation Matlab Software." *Experimental Mechanics* 55 (6): 1105–1122. https://doi.org/10.1007/s11340-015-0009-1.

Bui, Trung T., Ali Limam, Vasilis Sarhosis and Mohammed Hjiaj. 2017. "Discrete element modelling of the in-plane and out-of-plane behaviour of dry-joint masonry wall constructions." *Engineering Structures* 136: 277–294. https://doi.org/10.1016/j.engstruct.2017.01.020.

Canizzaro, Francesco and Paulo B. Lourenço. 2016. "Simulation of Shake Table Tests on Out-of-Plane Masonry Buildings. Part (VI): Discrete Element Approach." *International Journal of Architectural Heritage* 11 (1): 125–142. https://doi.org/10.1080/15583058.2016.1238973.

Cassar, JoAnn, Mario Galea, Reuben Grima, Katya Stroud and Alex Torpiano. 2011. "Shelters over the Megalithic Temples of Malta: debate, design and implementation." *Environmental Earth Sciences* 63: 1849–1860. https://doi.org/10.1007/s12665-010-0735-8.

Cassar, JoAnn, Shirley Cefai, Reuben Grima and Katya Stroud. 2018. "Sheltering archaeological sites in Malta: lessons learnt." *Heritage Science* 6: 36. https://doi.org/10.1186/s40494-018-0201-6.

Chen, Shipeng and Katalin Bagi. 2023. "DEM analysis of masonry hemispherical domes externally reinforced with metal bars." *Engineering Structures* 291: 116496. https://doi.org/10.1016/j.engstruct.2023.116496.

Cicilloni R. 2009. *I Dolmen della Sardegna*. Mogoro (OR), Italy: PTM Editrice. (in Italian).

Clemente, Paolo. 1998. "Introduction to dynamics of stone arches." *Earthquake Engineering and Structural Dynamics* 27 (5): 513–522. https://doi.org/10.1002/(SICI)1096-9845(199805)27:5<513::AID-EQE740>3.0.CO;2-O.

Comité Européen de Normalisation (CEN). 2006. *EN 1936:2006 Natural stone test methods - Determination of real density and apparent density, and of total and open porosity*. Bruxelles, BE: Comité Européen de Normalisation.

Comité Européen de Normalisation (CEN). 2007. *EN 1926:2007 Natural stone test methods - Determination of uniaxial compressive strength*. Bruxelles, BE: Comité Européen de Normalisation.

Cundall, Peter A. 1971. "Computer model for simulating progressive large-scale movements in blocky rock systems." *Proceedings of the Symposium of International Society of Rock Mechanics*, Nancy 1 (II-8).

de Felice Gianmarco. 2011. "Out-of-Plane Seismic Capacity of Masonry Depending on Wall Section Morphology." *International Journal of Architectural Heritage* 5 (4-5): 466–482. https://doi.org/10.1080/15583058.2010.530339.

DeJong, Matthew J. and Christopher Vibert. 2012. "Seismic response of stone masonry spires: Computational and experimental modeling." *Engineering Structures* 40: 566-574. https://doi.org/10.1016/j.engstruct.2012.03.001.De Santis Stefano and Gianmarco de Felice G. 2014. "A fibre beam based approach for the evaluation of the seismic capacity of masonry arches." *Earthquake Engineering and Structural Dynamics* 43 (11): 1661–1681. https://doi.org/10.1002/eqe.2416.

Dimitri, Rossana, Laura De Lorenzis and Giorgio Zavarise. 2011. "Numerical study on the dynamic behavior of masonry columns and arches on buttresses with the discrete element method." *Engineering Structures* 33 (12): 3172–3188. https://doi.org/10.1016/j.engstruct.2011.08.018.

Erdman, Arthur G., and George N. Sandor. 1984. *Mechanism Design: Analysis and Synthesis*. Englewood Cliffs, NJ, US: Prentice-Hall.

Ferrante, Angela, Dimitri Loverdos, Francesco Clementi, Gabriele Milani, Antonio Formisano, Stefano Lenci and Vasilis Sarhosis. 2021. "Discontinuous approaches for nonlinear dynamic analyses of an ancient masonry tower." *Engineering Structures* 230: 111626. https://doi.org/10.1016/j.engstruct.2020.111626.

Islam, M. Shariful and Benjamin J. Mohr. 2023. "Performance of clinoptilolite zeolite after milling as a pretreatment on hydration kinetics, shrinkage, and alkali-silica reaction of cementitious materials." *Cement* 12: 100069. https://doi.org/10.1016/j.cement.2023.100069.

Itasca. 2011. *UDEC - Universal Distinct Element Code. User's Guide Ver. 6.0*. Minneapolis, MN, US: Itasca Consulting Group, Inc.

Itasca. 2020. 3DEC - Three-Dimensional Distinct Element Code. User's Guide Ver. 7.0. Minneapolis, MN, US: Itasca Consulting Group, Inc.

Kassotakis, Nicko, Vasilis Sarhosis, Ajit Pillai and Lars Johanning. 2023. "Three-dimensional discrete element modelling of rubble masonry structures from geospatial data". In *Compdyn Proceedings of the 9th International Conference on Computational Methods in Structural Dynamics and Earthquake Engineering*, Athens, Greece: M. Papadrakakis, M. Fragiadakis (eds.).

Komodromos, Petros, Loizos Papaloizou and Panayiotis Polycarpou. 2008. "Simulation of the response of ancient columns under harmonic and earthquake excitations." *Engineering Structures* 30 (8): 2154–2164. https://doi.org/10.1016/j.engstruct.2007.11.004.

Lemos, José V. 2007. "Discrete element modelling of masonry structures." *International Journal of Architectural Heritage* 1: 190–213. https://doi.org/10.1080/15583050601176868.

Lemos, José V., and Alfredo Campos Costa. 2017. "Simulation of Shake Table Tests on Out-Of-Plane Masonry Buildings. Part (V): Discrete Element Approach." *International Journal of Architectural Heritage* 11 (1): 117–124. https://doi.org/10.1080/15583058.2016.1237587.

Lourenço, Paulo B, Daniel V Oliveira, Pere Roca and Augustin Orduña. 2005. "Dry Joint Stone Masonry Walls Subjected to In-Plane Combined Loading." *Journal of Structural Engineering* 131 (11): 1665‑1673. https://doi.org/10.1061/(ASCE)0733-9445(2005)131:11(1665).

Martínez-Torres, Luis M. 2017. "Building Materials of Neolithic Tombs in Alava, Northern Spain." *The Open Construction and Building Technology Journal* 11: 152–163. https://doi.org/10.2174/1874836801711010152.

Meletti, Carlo, Fabrizio Galadini, Gianluca Valensise, Massimiliano Stucchi, Roberto Basili, Salvatore Barba, Gianfranco Vannucci and Enzo Boschi. 2008. "A seismic source zone model for the seismic hazard assessment of the Italian territory." *Tectonophysics* 450 (1-4): 85–108. https://doi.org/10.1016/j.tecto.2008.01.003

Meriggi, Pietro, Gianmarco de Felice, Stefano De Santis, Francesca Gobbin, Anna Mordanova and Bartolomeo Pantò. 2019. "Distinct element modelling of masonry walls under out-of-plane seismic loading." *International Journal of Architectural Heritage* 13 (7): 1110–1123. https://doi.org/10.1080/15583058.2019.1615152.

Mordanova, Anna, and Gianmarco de Felice. 2020. "Seismic Assessment of Archaeological Heritage Using Discrete Element Method." *International Journal of Architectural Heritage* 14 (3): 345–357. https://doi.org/10.1080/15583058.2018.1543482.

Motsa, Siphesihle M., Georgios A. Drosopoulos, Maria E. Stavroulaki, Emmanuel Maravelakis, Ruben P. Borg, Pauline Galea, Sebastiano d'Amico and Georgios E. Stavroulakis. 2020. "Structural investigation of Mnajdra megalithic monument in Malta." *Journal of Cultural Heritage* 41: 96–105. https://doi.org/10.1016/j.culher.2019.07.004.

Mousavian, Elham, Bagi Katalin and Claudia Casapulla. 2023. "Torsion–Shear Behaviour at Interlocking Joints: Calibration of Discrete Element-Deformable Models Using Experimental and Numerical Analyses." *International Journal of Architectural Heritage* 17 (1): 212–229. https://doi.org/10.1080/15583058.2022.2101034.

Oliveira, Daniel V., Giulia Grecchi, A. McCall, Jungtae Noh, E. Speer and M. Tohidi. 2012. "Seismic analysis of the Roman Temple of Évora, Portugal." In *Proceedings of the 15th World Conference on Earthquake Engineering*, Lisbon, Portugal.

Oppenheim, Irving J. 1992. "The masonry arch as a four-link mechanism under base motion." *Earthquake Engineering and Structural Dynamics* 21: 1005–1017. https://doi.org/10.1002/eqe.4290211105.

Papantonopoulos, C. Ioannis N. Psycharis, D.Y. Papastamatiou, Jose V. Lemos, and H.P. Mouzakis. 2002. "Numerical prediction of the earthquake response of classical columns using the distinct element method." *Earthquake Engineering and Structural Dynamics* 31 (9): 1699-1717. https://doi.org/10.1002/eqe.185.

Pappas Athanasios, Francesca da Porto and Claudio Modena. 2016. "Seismic Vulnerability Assessment Form for Free-Standing Columns Based on a Simplified Numerical Analysis". *International Journal of Architectural Heritage* 10 (2-3): 281–299. http://dx.doi.org/10.1080/15583058.2015.1113336.

Pulatsu, Bora, Eduardo M. Bretas and Paulo B. Lourenço. 2016. "Discrete element modeling of masonry structures: Validation and application." *Earthquakes and Structures* 11 (4): 563–582. https://doi.org/10.1016/10.12989/eas.2016.11.4.563.

Pulatsu, Bora, Semih Gonen, Ece Erdogmus, Paulo B. Lourenço, Jose V. Lemos and Ravi Prakash. 2021. "In-plane structural performance of dry-joint stone masonry Walls: A spatial and non-spatial stochastic discontinuum analysis." *Engineering Structures* 242: 112620. https://doi.org/10.1016/j.engstruct.2021.112620.

Reinosa, Jose M. and Luis E. Romera. 2015. "Stability of megalithic structures against overturning." *Journal of Cultural Heritage* 16 (6): 798–804. https://doi.org/10.1016/j.culher.2015.03.006.

Salvalaggio, Matteo, Jacopo Bonetto, Matteo Zampar and Maria Rosa Valluzzi. 2021. "Numerical Prediction of the Seismic Behavior of Reassembled Columns in Ancient Structures: An Anastylosis Model for the Temple of Apollo Pythios in Gortyn (Crete)." *Heritage* 4: 3421–3441. https://doi.org/10.3390/heritage4040190.

Sarhosis, Vasilis, Daniele Baraldi, José V. Lemos and Gabriele Milani. 2019. "Dynamic behaviour of ancient freestanding multi-drum and monolithic columns subjected to horizontal and vertical excitations." *Soil Dynamics and Earthquake Engineering* 120: 39–57. https://doi.org/10.1016/j.soildyn.2019.01.024.

Torpiano, Alex. 1995. "The collapse and proposed restoration of a prehistoric megalithic structure." *WIT Transactions on The Built Environment* 15: 237–244.

Türer, Ahmet, Yasemin D.A. Erdem and Neriman Ş Güçhan. 2012. "Reverse-Engineering Evaluation and Monitoring of Nemrut Monuments." *International Journal of Architectural Heritage* 6 (4): 373–395. https://doi.org/10.1080/15583058.2011.561906.

Young, Meagan P., Arturo E. Schultz, and José V. Lemos. 2015. "Seismic analysis of the panhellenic sanctuary of Nemea, Greece." In *Proceedings of the 12th North American Masonry Conference*. Denver, CO, US: The Masonry Society.

Figure 1. *Sa Covaccada* Dolmen: pictures taken in 2010 (before restoration) of outside front view (a), inside view of the capstone (b), outside view of the east orthostat (c) and outside view of the west orthostat (d), and pictures taken in 2023 (after restoration) of the front view (e), and outside view of the west orthostat (detail, f).

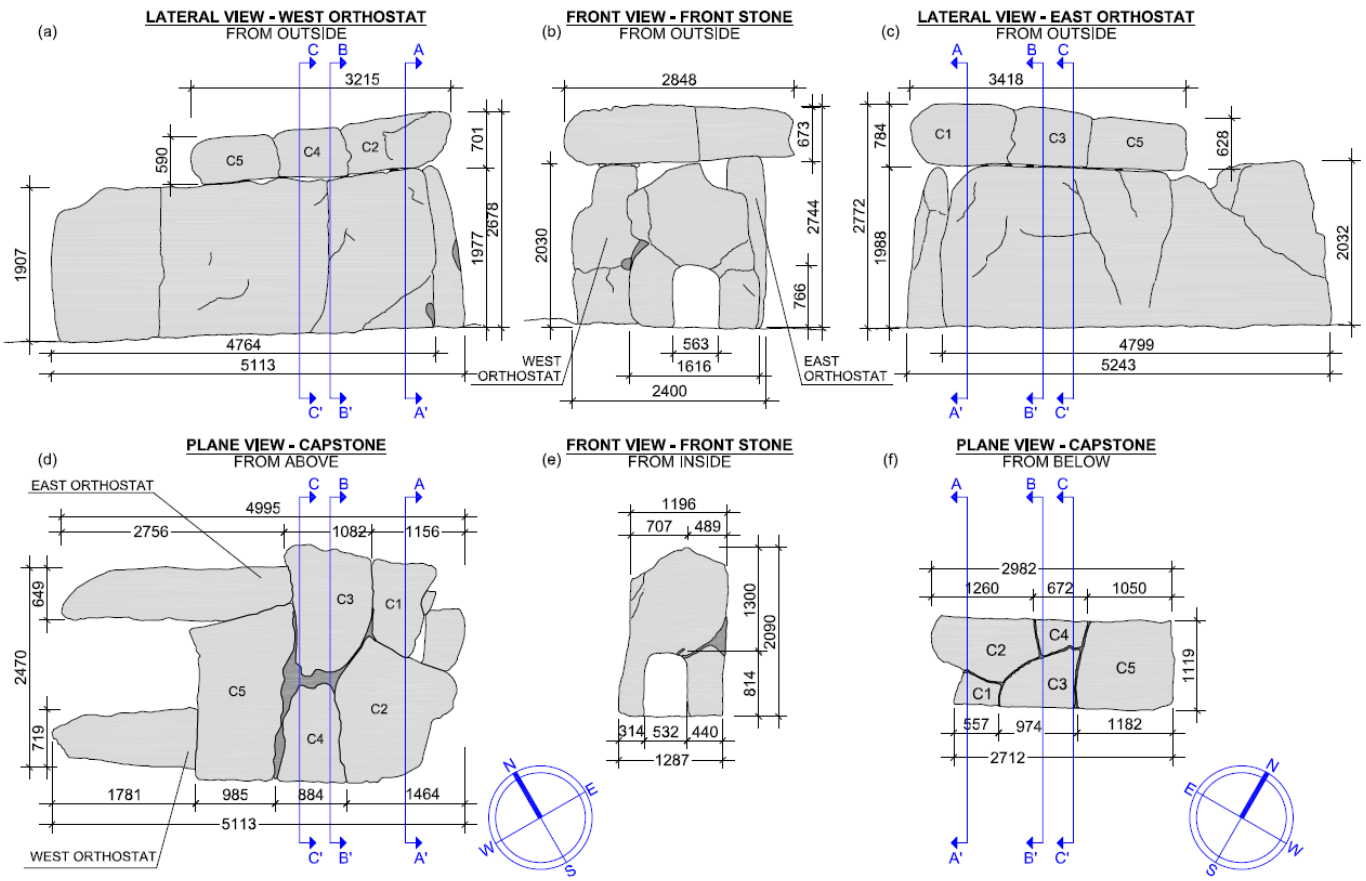

Figure 2. Geometric survey and crack pattern of *Sa Covaccada* Dolmen.

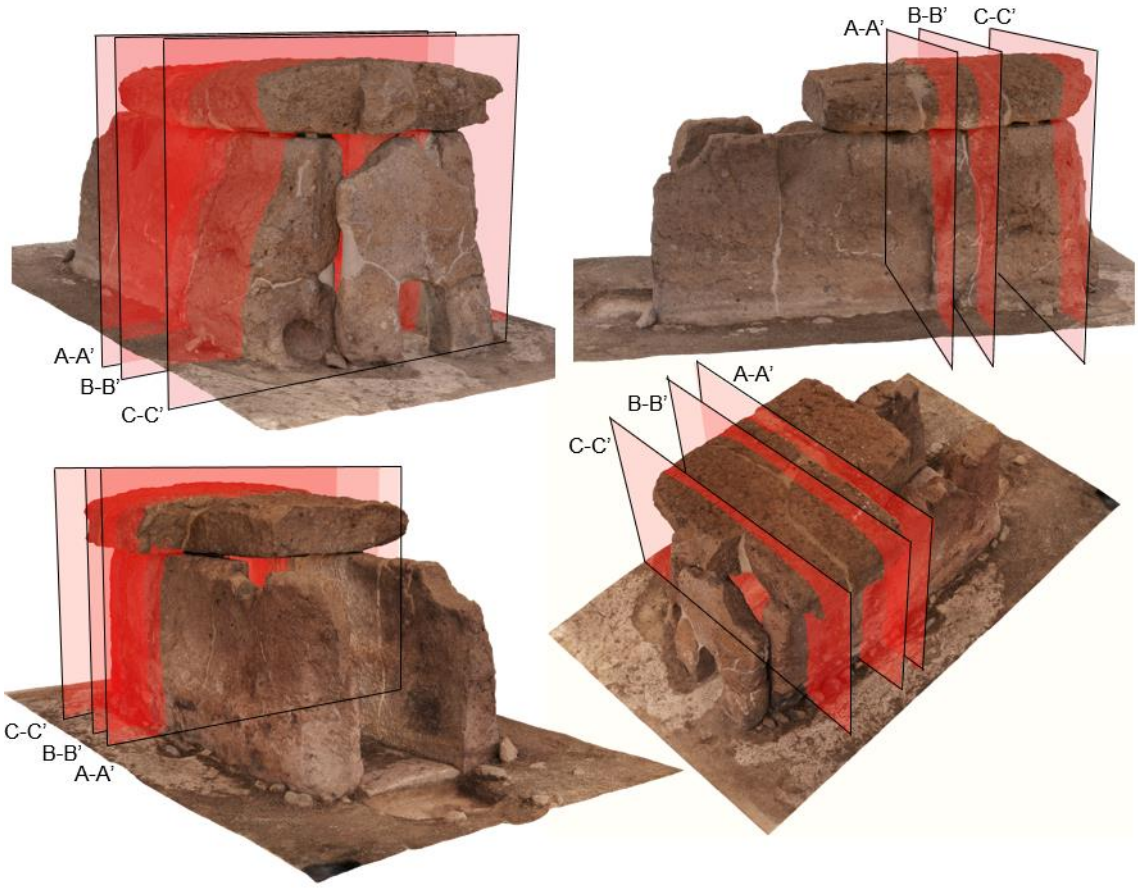

Figure 3. 3D geometric model from laser scan and digital photogrammetry survey and cross-section planes (Esplorativa Architetti, Torino, Italy).

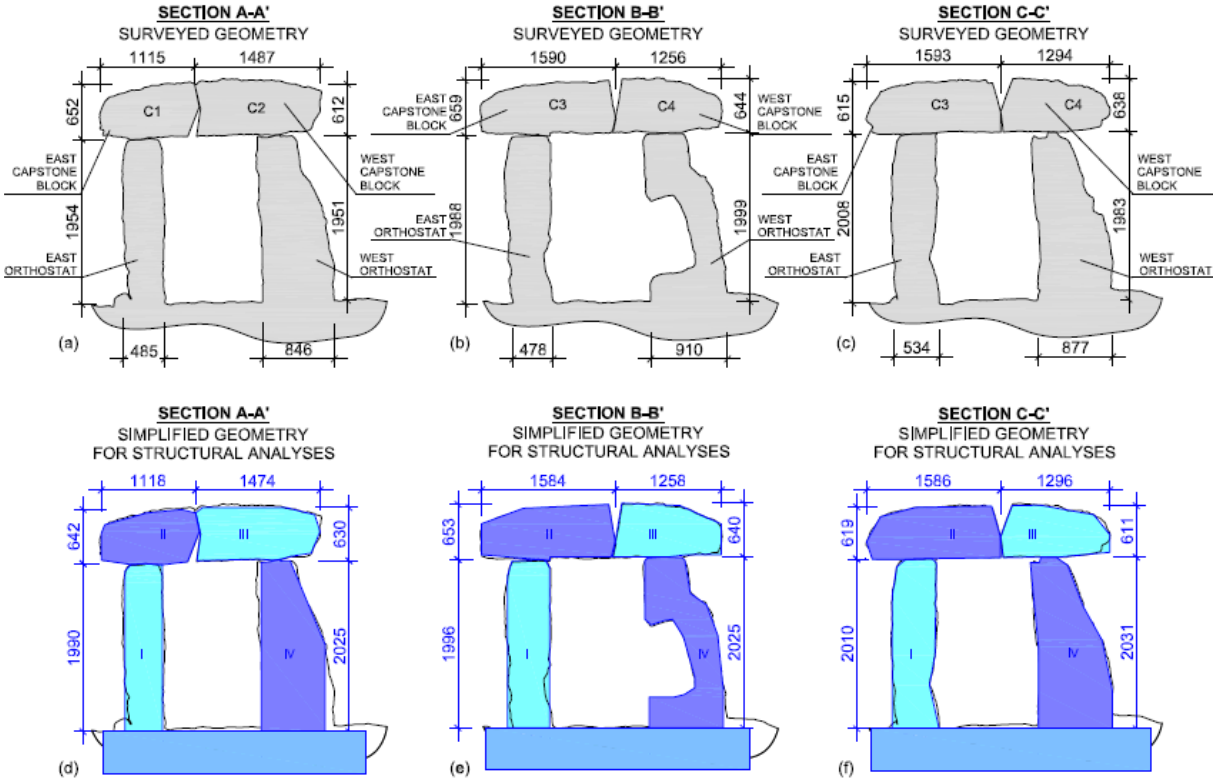

Figure 4. Cross-sections A-A' (a,d), B-B' (b,e), and C-C' (c,f), extracted from surveyed 3D geometric model (a-c) and corresponding simplified geometry for structural analyses (d-f).

Figure 5. Stone sample collected in the field (a), cubic specimen extracted with numerically controlled milling machine (b), experimental setup for compression tests and damage state of one specimen at failure (c) and vertical displacement field calculated with Digital Image Correlation (d).

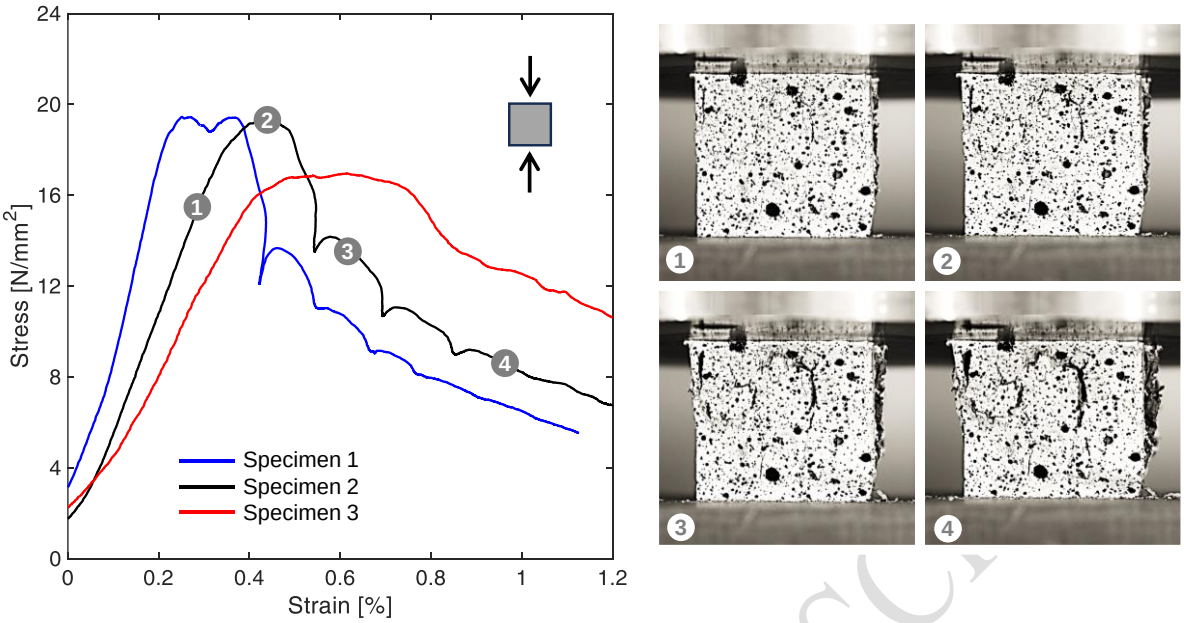

Figure 6. Axial stress versus axial strain response curves of compression tests on stone cubic specimens and progressive crack pattern.

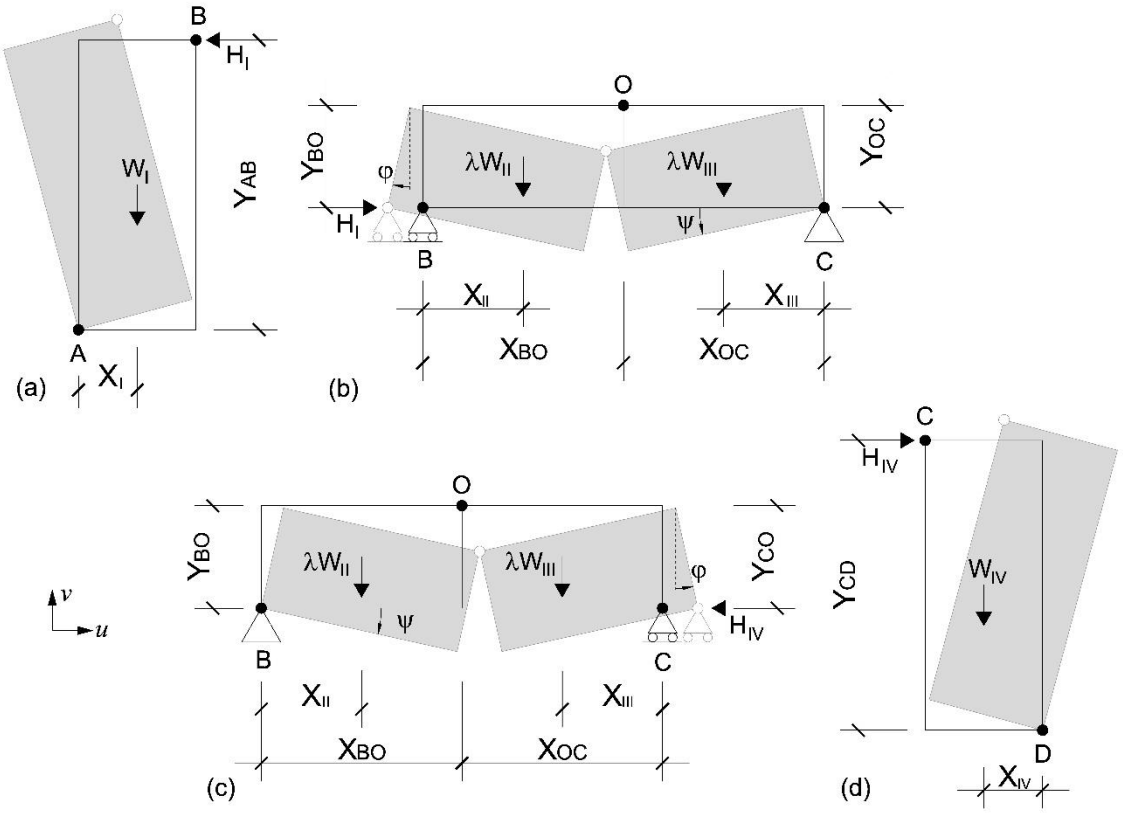

Figure 7. Schemes of the rigid body mechanisms involving the east orthostat and the capstone (a-b, east mechanism) and the capstone and the west orthostat (c-d, west mechanism).

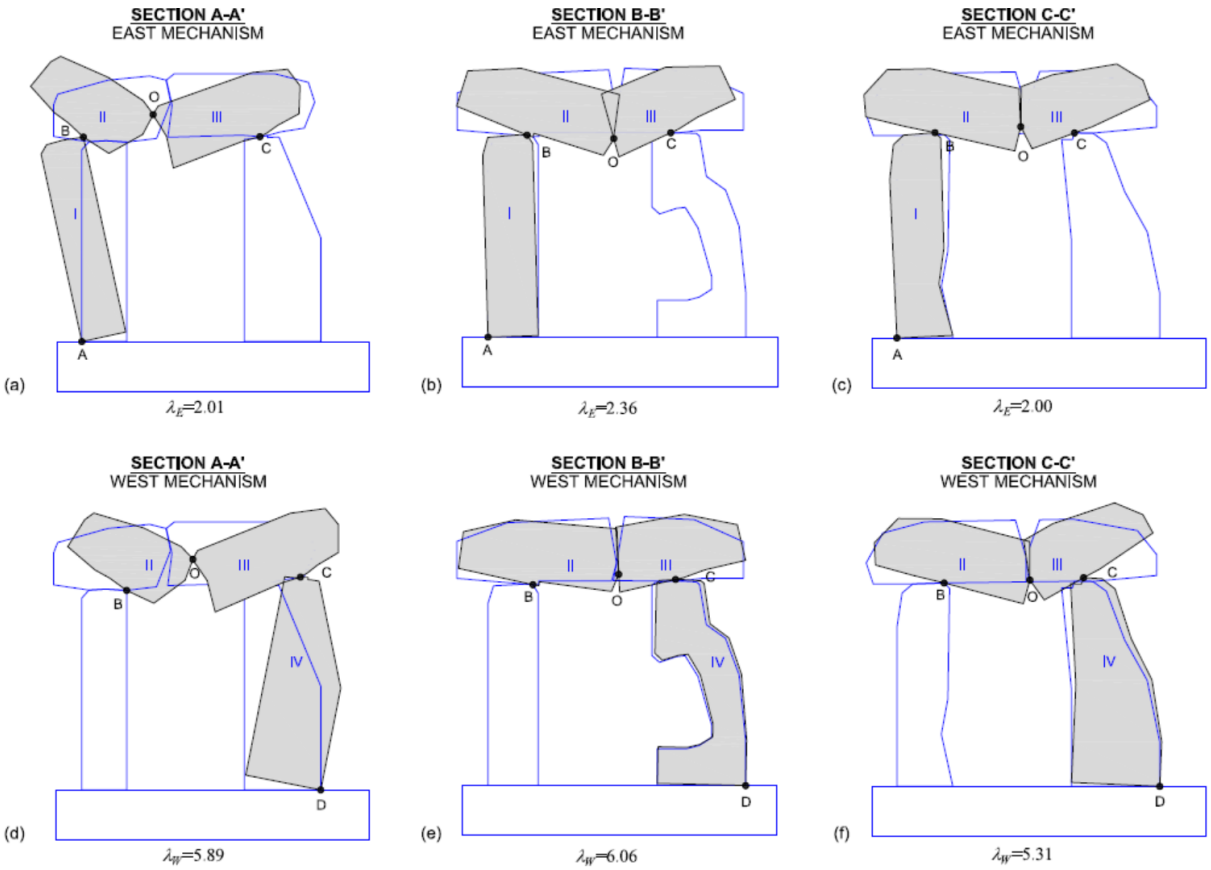

Figure 8. East (a-c) and west (d-f) mechanisms considered for rigid block analyses of cross-sections A-A' (a,d), B-B' (b,e), and C-C' (c,f) (deformed configurations based on virtual displacements).

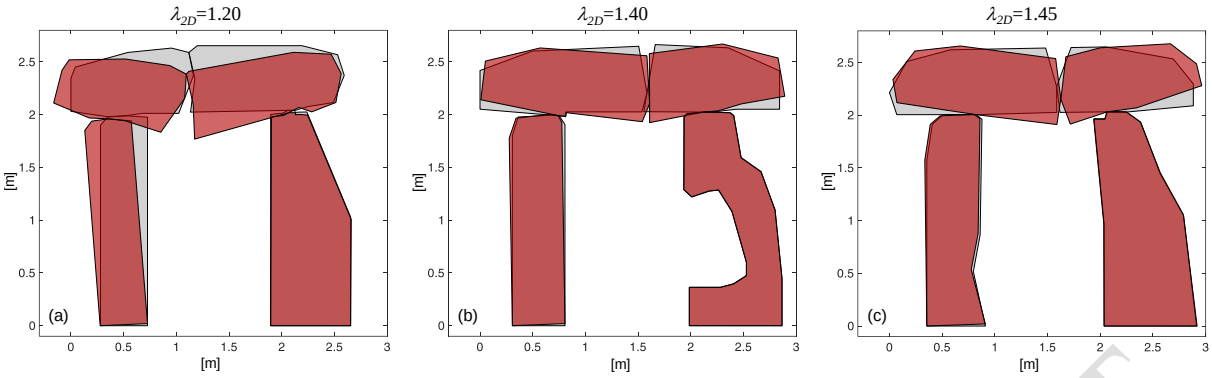

Figure 9. Collapse mechanisms identified by 2D DEM simulations for sections A-A' (a), B-B' (b), and C-C' (c) (displacements amplified by 10).

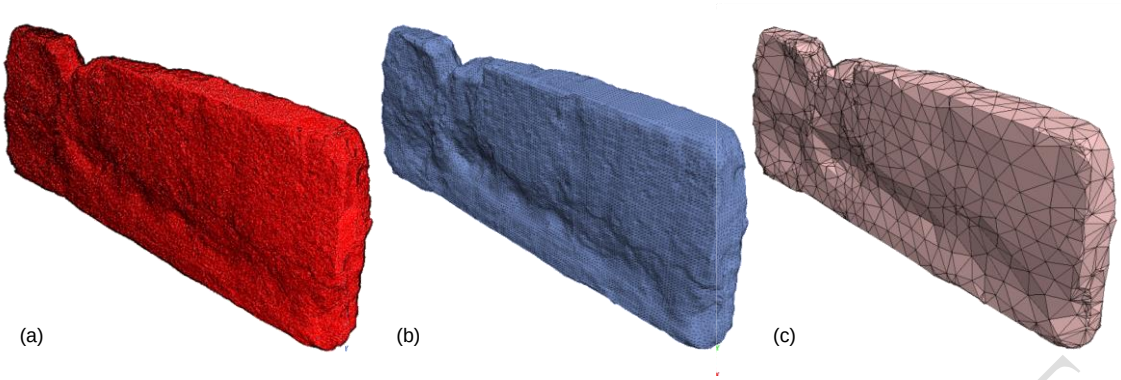

Figure 10. Geometrical pre-processing for 3D DEM analyses: STL geometric model from digital survey (a), enveloped and meshed blocks in Autodesk Meshmixer® CAD environment (b), and meshed units in 3DEC® (c) of the east orthostat.

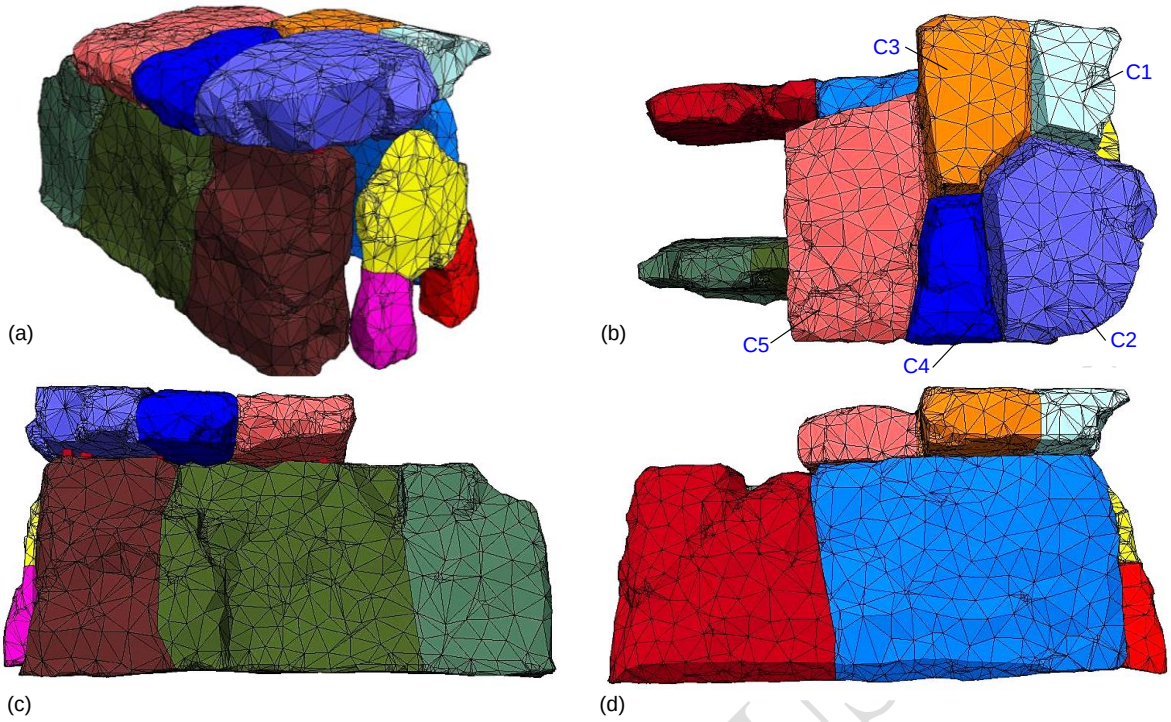

Figure 11. Numerical model for 3D DEM analyses (3DEC®): overview (a), plan view of the capstone (b), and lateral views of the west (c) and of the east (d) orthostats.

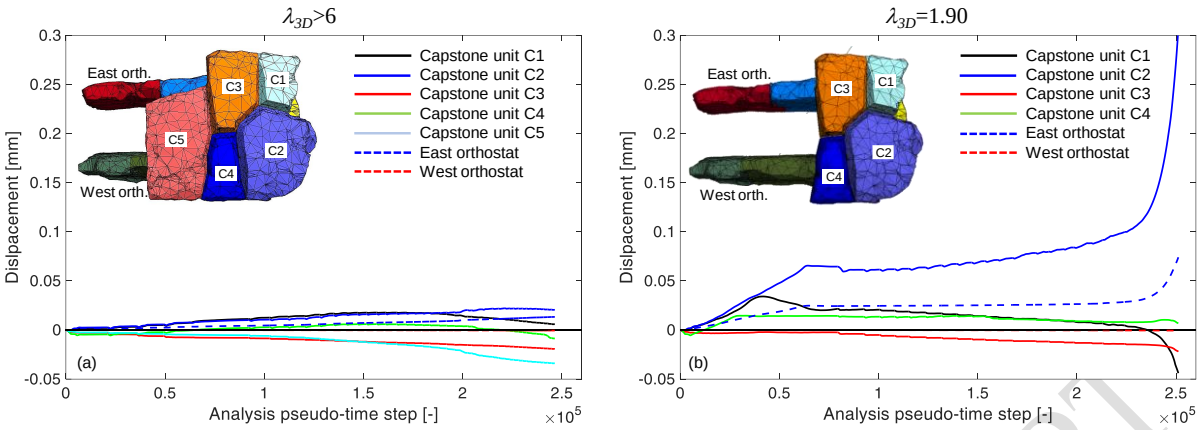

Figure 12. Displacements of capstone units and orthostats during 3D DEM simulations for the complete model (a) and for the partial model (capstone block C5 removed, b).

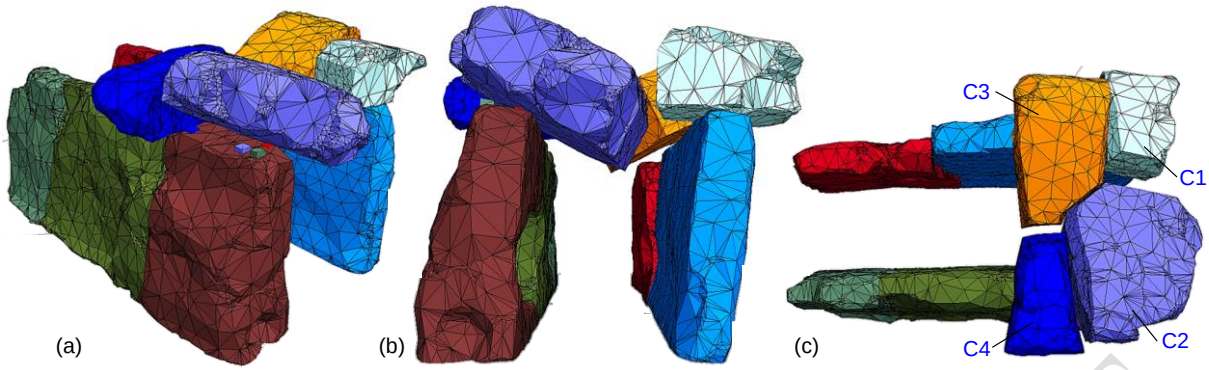

Figure 13. Collapse mechanism identified by 3D DEM simulations (capstone block C5 removed).

Table 1. Collapse multipliers.

Section	Mechanism analyses		2D DEM analyses	3D DEM analyses
	λ_E	λ_W	λ_{2D}	λ_{3D}
A-A’	2.01	5.89	1.20	>6
B-B’	2.36	6.06	1.40	
C-C’	2.00	5.31	1.45	

Table 2. Thickness and self-weight density of the blocks defined for 2D DEM analyses.

Cross-section	Thickness and block self-weight density			
	I	II	III	IV
A-A’	4.86m / 8756.8kN/m^2	0.81m / 1449.9kN/m^2	1.54m / 2777.8kN/m^2	4.82m / 8675.2kN/m^2
B-B’	4.86m / 8756.8kN/m^2	1.28m / 2308.0kN/m^2	1.33m / 2402.7kN/m^2	4.82m / 8675.2kN/m^2
C-C’	4.86m / 8756.8kN/m^2	1.28m / 2308.0kN/m^2	1.33m / 2402.7kN/m^2	4.82m / 8675.2kN/m^2